

# Simulated future changes of extreme nutrient loads in a mesoscale agricultural watershed in Bavaria

## Simulierte zukünftige Änderungen der Extremwerte für Nährstofffrachten in einem mesoskaligen landwirtschaftlichen Einzugsgebiet in Bayern

Bano Mehdi<sup>1, 2\*</sup>, Ralf Ludwig<sup>3</sup>, Bernhard Lehner<sup>4</sup>

<sup>1</sup> University of Natural Resources and Life Sciences, Vienna (BOKU), Department of Crop Sciences, Division of Agronomy, 3430 Tulln, Austria

<sup>2</sup> University of Natural Resources and Life Sciences, Vienna (BOKU), Institute of Water Management, Hydrology and Hydraulic Engineering, 1190 Vienna, Austria

<sup>3</sup> Ludwig Maximilians University, Department of Geography, 80333 Munich, Germany

<sup>4</sup> McGill University, Department of Geography, Montreal, QC, H3A 0B9, Canada

\* Corresponding author: bano.mehdi@boku.ac.at

Received: 29 January 2016, received in revised form: 4 February 2016, accepted: 5 February 2016

### Summary

The hydrological model SWAT was applied to the upper Altmühl watershed to examine the simulated 10<sup>th</sup> and 90<sup>th</sup> percentiles of streamflow, nitrate nitrogen (NO<sub>3</sub><sup>-</sup>-N), and total phosphorus loads (TP), using an ensemble of reference climate (1975–2000) and future climate (2046–2070) simulations. A comparison between the two periods showed that in the future, the 90<sup>th</sup> percentiles of the NO<sub>3</sub><sup>-</sup>-N loads increase in all seasons which indicates a trend to increasing diffuse pollution in the mid-term future. Conversely, the 90<sup>th</sup> percentile TP loads diminished in winter and otherwise remained similar to the reference period. The 10<sup>th</sup> and 90<sup>th</sup> percentile changes in the future streamflow followed changes in precipitation, and did not have any apparent influence on extreme nutrient transport events.

**Keywords:** hydrological modeling, nutrient transport, climate change, nitrogen and phosphorus concentrations, 10<sup>th</sup> and 90<sup>th</sup> percentiles

### Zusammenfassung

Das hydrologische Modell SWAT wurde im Altmühl-Einzugsgebiet angewendet, um die 10. und 90. Perzentile der Abfluss, Nitrat-Stickstoff (NO<sub>3</sub><sup>-</sup>-N) und Gesamtphosphor (TP) für Ensembles von Referenz- (1975-2000) und zukünftige (2046-2070) Klimabedingungen zu simulieren. Der Vergleich zwischen den Ensemble-Simulationen in beiden Zeiträumen zeigt, dass die 90. Perzentile der NO<sub>3</sub><sup>-</sup>-N Frachten in allen Jahrzeiten in der Zukunft signifikant erhöht waren. Dies deutet darauf hin, dass Stickstoff einen größeren Einfluss auf Frachttransporte in der mittelfristigen Zukunft in dem Altmühl Einzugsgebiet haben könnte. Umgekehrt waren die 90. Perzentile der TP Frachten im Winter verringert und ansonsten ähnlich wie im Referenzzeitraum. Die Veränderungen der 10. und 90. Perzentile für den Abfluss unter zukünftige Klimabedingungen folgten den Niederschlagsänderungen und hatten keinen eindeutigen Einfluss auf die extrem Nährstofftransportereignisse.

**Schlagworte:** hydrologische Modellierung, Nährstofftransport, Klimawandel, Stickstoff- und Phosphor-Konzentrationen, 10. und 90. Perzentile

## 1. Introduction

The impacts of climate change on large nutrient transport events are not well-studied, even though in agricultural regions, nutrients applied as fertilizer can be lost from row crops more readily in the future as soil loss is enhanced through higher precipitation amounts and greater intensities (Michael et al., 2005; Hancock, 2012).

For example, in western Germany, since 1950, heavy and extreme precipitation events (95<sup>th</sup> and 99<sup>th</sup> percentiles) increased by 5–13% per decade in winter, spring, and autumn, and showed decreasing tendencies of 3–9% per decade during summer (Zolina et al., 2008). Heavy precipitation trends have been simulated to continue in the future for Germany, with winter projected to have a greater increase in extreme precipitation than summer (Radermacher and Tomassini, 2012). Such changes will affect the nutrient transport to surface waters. A study in vineyards in Spain showed that large precipitation and runoff events transported the highest annual nutrient loads into the surface water bodies (Ramos and Martínez-Casasnovas, 2009).

In Europe, achieving a good qualitative and quantitative status for water bodies to a near-term horizon of 2027 is a challenge currently being addressed by the European Water Framework Directive (EC, 2000). Therefore, extreme nutrient transport events must be investigated to evaluate how they may be expected to change in the future. The mean transport or load of nutrients in a stream is the result of the sum of all point and diffuse inputs, minus the sum of all nutrient retention and losses (Behrendt and Opitz, 2000). The objective of the study was to quantify the changes in 10<sup>th</sup> and 90<sup>th</sup> percentiles in streamflow, nitrate nitrogen ( $\text{NO}_3^-$ -N), and total phosphorus (TP) loads under climate change conditions to 2046–2070 (a mid-term time horizon) compared with a reference period of 1975–2000. For this, a hydrological model was used. Hydrological models are tools consisting of mathematical equations that can simulate the physical processes in a watershed, which lead to nutrient load losses at the outlet.

The Altmühl watershed was investigated as water quality problems in the Altmühl River and Lake persist due to diffuse inputs causing elevated phosphorus (P) levels. The P concentrations are linked to the cyanobacterial outbreaks in the lake (Schrenk-Berger et al., 2004). Since 1982, water quality improvements in the Altmühl River and Lake have been observed mainly by reducing the point source inputs, by conducting upgrades to water treatment plants and storm water treatment facilities as well as introducing environmental regulations (i.e., limiting phosphates con-

tained in detergents). Also, from 1990–1996, measures were undertaken to reduce surface runoff, which included the creation of hedges, field buffer strips, and stream bank re-vegetation along 200 km (BMLU, 2002). Nevertheless, the TP concentrations in the river and lake often exceed the government guidelines of 0.05 mg/L and are measured at 0.3 and 0.2 mg/L, respectively (BMLU, 2002).

## 2. Materials and Methods

### 2.1 Description of the study watershed

Figure 1 shows the location of the upper part of the Altmühl watershed in Germany, which encompasses a total basin area of 980 km<sup>2</sup> and includes 130 km of river length from the source of the Altmühl to the gauge in Treuchtlingen (10°54'48.91"E, 48°57'11.31"N). The Treuchtlingen gauge is the outlet in this study. The elevation ranges from 660 m to 406 m at the outlet. The soils in the upper part of the study area are mainly loamy clay and loamy gravelly sand, with pockets of gravelly sand. Below the Altmühl Lake are mainly clayey silt soils along the floodplain. Clay loam soils are predominant near the outlet, with a few areas of Karst in the most south-western tip of the basin. The watershed consists primarily of agricultural (60%), forested (30%), and urban areas (5%). Detailed field data available from the Bavarian State Office for Agriculture, show the agricultural land in 2008 to be mainly winter and summer cereals (26,065 ha), pasture (24,620 ha), maize (7942 ha), rape (2690 ha), alfalfa and clover (1369 ha) with pockets of other vegetable and fruit crops (Table 1). The Altmühl watershed receives approximately 700 mm of precipitation annually. Evapotranspiration is 475 mm and runoff in the basin is 175 mm (StLFW, 1996), the remaining 50 mm is most likely lost to deep aquifer recharge due to the Karst areas in the southern watershed.

### 2.2 The hydrological model SWAT

The hydrological model Soil and Water Assessment Tool (SWAT; Arnold et al., 1998) was applied to the watershed to examine streamflow, as well as  $\text{NO}_3^-$ -N and TP loads for both a historic and a future period. SWAT was developed by the United States Department of Agriculture to reflect the impacts of agricultural management practices on streamflow, agricultural nutrient, and sediment yields in surface waters. SWAT is a semi-distributed, process-based hydrological model run on a daily time step (Gassman et

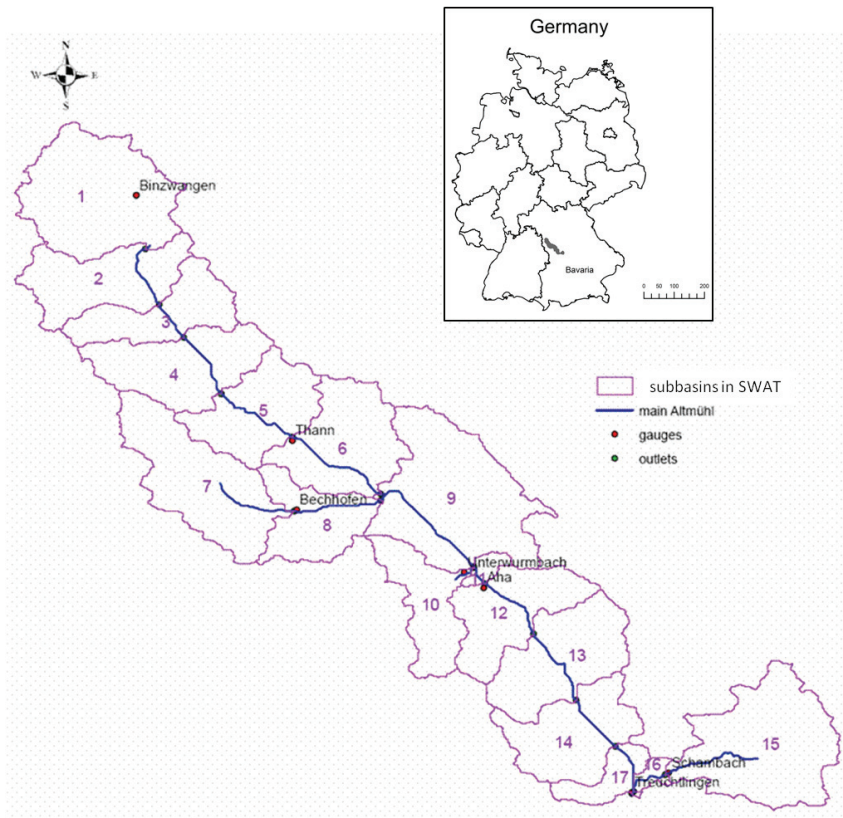


Figure 1. Location of the Altmühl watershed in Germany and the setup in SWAT of the upper Altmühl River.  
Abbildung 1. Die Lage des Altmühl-Einzugsgebietes in Deutschland sowie die Darstellung des oberen Altmühl-Einzugsgebietes im Rahmen von SWAT.

al., 2007; Arnold et al., 2012). SWAT uses the concept of hydrological response units (HRUs) to model the hydrological processes in the watershed. HRUs are areas of similar land use, soil, and slope in each sub-basin.

ArcSWAT version 510 was run on an ArcGIS 9.3.1 (ESRI 2009, California, USA) platform. The setup for the watershed was based on a 50 m Digital Elevation Model.

In SWAT, the simulated processes include infiltration, surface runoff, evaporation, plant water uptake, lateral flow, and percolation to shallow and deep aquifers. Flow, sediment, and nutrients are summed across the HRUs in a sub-basin, and the flows and pollutant loads are then routed through channels, ponds, and reservoirs to the watershed outlet. The volume of surface runoff is estimated using the modified SCS curve number (CN) method (USDA, 1972), which takes into account precipitation, abstractions, and soil storage; the lower the CN, the more permeable the surface. The CN is adjusted at each time step, depending on how much soil moisture is available. The potential evapotranspiration was estimated using the Penman–Monteith method.

The crop growth was modeled with the EPIC sub-model (Williams et al., 1984) that bases the phenological development of the plant on the accumulated plant heat units (PHUs), which are a function of the minimum and maximum air temperatures.

The SWAT model has three major forms of nitrogen that it models in mineral soils: (1) the organic pool associated with humus, (2) a plant-available pool in the soil solution, and (3) an insoluble inorganic component (Neitsch et al., 2011). There are five main pools associated with these nitrogen forms: two inorganic pools ( $\text{NH}_4^+$  and  $\text{NO}_3^-$ ) and three organic pools (fresh plant residue, stable humic substances, and active humic substances). For details of the transformation processes, see Neitsch et al. (2011).

In SWAT, the P cycle contains three major sources of P in mineral soils: the organic pool associated with humus, a plant-available pool in the soil solution, and an insoluble inorganic component.

SWAT models six different pools of P in the soil; three pools are associated with the inorganic forms of P (solution, active, and stable) and the other three with the or-

Table 1. Land use in the upper Altmühl watershed for 2008. The general land use data stems from the Bavarian State Office for the Environment, the agricultural land use data source is the Bavarian Regional Office for Agriculture.

Tabelle 1. Die Landnutzung im oberen Altmühl-Einzugsgebiet für das Jahr 2008. Die allgemeinen Landnutzungsdaten stammen vom Bayerischen Landesamt für Umwelt, die Daten zur landwirtschaftlichen Nutzung wurden vom Bayerischen Landesamt für Ernährung, Landwirtschaft und Forsten zu Verfügung gestellt.

Dominant land use type	SWAT Code	Area in watershed	
		(ha)	(%)
Forest	FRST	29296.75	29.5
Pasture land	PAST	24619.75	24.8
Winter cereals (wheat, barley, rye, triticale)	WWHT	20174.25	20.3
Maize (silage)	CSIL	7589.5	7.6
Summer cereals (wheat, barley, rye, oats, spelt)	SWHT	5890.75	5.9
Rape, sunflower	CANA	2690.25	2.7
Alfalfa, clover	ALFA	1396.25	1.4
Maize (grain)	CORN	352.5	0.35
Sugarbeet, asparagus	SGBT	219.25	0.22
Potatoes	POTA	166.75	0.17
Beans, peas	SOYB	136.5	0.14
Orchard	ORCD	29.25	0.03
Miscanthus	SWCH	22.75	0.02
Strawberries	STRW	10.5	0.01
Land taken out of productivity	RNGB	456.75	0.46
Urban areas	URML	5549.25	5.59
Surface water bodies	WATR	740.5	0.75

ganic P forms (fresh, stable, and active). The fresh organic pool is associated with the crop residues and microbial biomass. The active and stable organic P pools are both associated with the soil humus, which is partitioned into these two pools to allow for the P to transform from humic substances to mineralized substances. The P mineralization algorithms are net mineralization algorithms, which take into account immobilization.

The inorganic P in solution is the available form of P that plants can take up. This pool is in rapid equilibrium with the active pool. The primary movement of soluble P in the soil is by diffusion due to a concentration gradient in the soil. Organic and inorganic P may be transported through the attachment to soil particles. The details of the processes are provided in Neitsch et al. (2011).

### 2.2.1 Data sources

The necessary observed climate data was provided by the German Meteorological Service (Deutscher Wetterdienst, 2011) and included the measured temperature, precipitation, relative humidity, cloud cover, and hours of sunshine.

Observed daily flows from 1981–2010 at the Thann gauge (basin area of 326.7 km<sup>2</sup>), from 1975–2010 at the Aha gauge (basin area of 689.4 km<sup>2</sup>), and from 1948–2006 at the Treuchtlingen gauge were available from the Water Management Authority in Ansbach. The measured monthly in-stream NO<sub>3</sub><sup>-</sup>-N and TP concentrations from the Bavarian State Office for the Environment were only available from 1982–2011 at the Thann gauge. The baseflow filter program (Arnold and Allen, 1999) was applied to the streamflow records from these gauges to determine the groundwater recharge and establish the baseflow recession constant for SWAT.

The general land use data was obtained from the Bavarian State Office for the Environment and data for the agricultural land use came from the Bavarian Regional Office for Agriculture. Soil parameter data was acquired from the GLOWA-Danube project (Muerth, 2008) and the Bavarian State Office for Agriculture (Wendland et al., 2011). Data on crop seeding, tillage, and fertilization application dates and amounts, as well as crop harvesting dates were gathered from the Bavarian State Office for Agriculture annual crop reports, and from the Association for Technology and Struc-

tures in Agriculture (KTBL, 1995; KTBL, 2009). Data on soil conservation practices in the watershed were guided by the responses received from a research questionnaire, in which 30% of the farmers in the surveyed area indicated they implement no-till or reduced tillage practices. The land use layer from 2008 remained static in the modeling study (i.e., no crop rotations were implemented from year to year).

### 2.3 Climate simulation ensembles

A suite of RCM data generated by the Ouranos Consortium on Regional Climatology and Adaptation to Climate Change was available for this research (Velázquez et al., 2013). Each simulation from the RCM was driven by a coupled GCM for the time periods 1970–2000 and 2041–2070. In total, seven coherent sets of climate variables of temperature, precipitation, relative humidity, solar radiation, and wind speed were available to drive the SWAT hydrological model (Figure 2). The regional climate models were: Rossby Centre Regional Atmospheric Climate Model (RCA), Regional Atmospheric Climate Model (RAC), Canadian Regional Climate Model (CRC). The driving Global climate models were: Bergen Climate Model (BCM), ECHAM (ECM) version 5 (members 1, 2 and 3), and Hadley Centre Coupled Model (HCM), and Canadian General Circulation Model (CGC).

The global climate models had the A1B greenhouse gas emission SRES projection (Nakicenovic et al., 2000), except for the CGC, which used the A2 scenario. Both of these SRES represent the higher greenhouse gas contribution scenarios. The A1B scenario has CO<sub>2</sub> emissions peaking around 2050, at 16 GtC and fall to about 13 GtC by 2100. In the A2 scenario, the global CO<sub>2</sub> emissions reach 29 GtC by 2100. The 1990 global CO<sub>2</sub> emissions were 6 GtC.

Temperature for each member of the ensemble was bias-corrected using a monthly correction factor based on the difference between the ensemble mean of the 30-year mean monthly minimum and maximum air temperature and the 30-year monthly means of the daily-observed minimum and maximum air temperatures. A bias-correction method for precipitation was applied to all climate simulations using the Local Intensity Scaling (Schmidli et al., 2006) at a sub-daily time step. Finally, the RCM outputs were scaled to a finer resolution of a 1 km grid with the scaling tool SCALMET (Marke, 2008), which preserves energy and mass at the scale of the RCM grid. For more detailed explanations of the climate simulations post-processing, see Muerth et al. (2013).

### 2.4 SWAT calibration and quantification of modeling uncertainty

A semi-automated inverse modeling procedure called Sequential Uncertainty Fitting algorithm (SUFI-2) version 4.3.2 (Abbaspour, 2011) was used for calibrating the SWAT-simulated outputs to the available time series data of streamflow, NO<sub>3</sub><sup>-</sup>-N, and TP loads. SUFI-2 is a stochastic procedure, drawing independent parameter sets using Latin Hypercube Sampling (LHS). For a detailed description of SUFI-2 procedures, see Abbaspour et al. (2004).

The SWAT model was calibrated sequentially, at the yearly, monthly, and daily time steps, for streamflow, NO<sub>3</sub><sup>-</sup>-N, and TP (Arnold et al., 2012). SWAT was first calibrated (1964–1974) at the outlet gauge (Treuchtlingen) for surface flow (validated from 1975–1984). Subsequently, NO<sub>3</sub><sup>-</sup>-N, and TP were calibrated (1982–1983) at the monthly time step at the Thann gauge (and validated in 1984). The SWAT model was set up to meet the satisfactory objective criteria listed in Moriasi et al. (2007), whereby the Nash-Sutcliffe efficiency (NS) was used as the main objective function. The details of the calibration are presented in Mehdi et al. (2015).

The available observed station data and simulated climate data were used from 1970–2000 (“reference period”), and 2041–2070 (“future period”), respectively. However, a 5-year warm up period was removed from all SWAT simulations; therefore, outputs were examined and presented from 1975–2000 and 2046–2070, respectively.

All climate simulations were bias-corrected, which allowed a direct comparison to be made between the SWAT simulations using the observed climate and using the future climate simulations. However, to remove the errors brought about by the SWAT model, as well as by the climate models, comparisons were made from SWAT outcomes using the climate simulations from the reference period and SWAT outcomes using the future climate simulations.

Once the SWAT model was set up, it was run with input from the observed station climate data from 1970–2000. Next, all else remaining the same, SWAT was run in turn with each of the climate simulations from the reference period, by replacing the observed climate. The SWAT model was subsequently run with each of the climate simulations for the future period. The output variables examined were always streamflow, NO<sub>3</sub><sup>-</sup>-N, and TP.

Independent t-tests were carried out ( $p < 0.05$ ) between the output variables (by season) simulated from the reference and the future period.

### 3. Results and discussion

#### 3.1 Future changes in temperature and precipitation

The climate by the end of the century in Germany is simulated to be warmer, and there will be a noticeable increase in extremes in Europe, such as heat waves, droughts, and precipitation events (Kovats et al., 2014). The climate simulations used in this study showed increases in the mean monthly temperatures ranging from 0.5 to 4 °C with most of the models agreeing on the greatest warming occurring in winter and in summer months (Figure 2a).

The simulated precipitation for most months was higher than in the reference period, especially during December to April, by up to 50%. The months of August and September showed a decrease in precipitation, of up to 80% in August (Figure 2b). Overall, the average annual precipitation in the observed reference period was 705.3 mm, whereas in the future period, the mean of the climate simulations showed this amount to be 752.3 mm. The month with the greatest increase in precipitation for the future was April with an additional 10 mm (average of seven climate simulations).

#### 3.2 Evaluating the SWAT model performance

After the calibration and validation steps, SWAT was able to reproduce the timing of daily dry spells and peak flows. The magnitude of flow events was also modeled satisfactorily, but SWAT tended to underestimate the overall flow (PBIAS = 13.8%), especially for the lower streamflow between runoff events. The calibration and validation of SWAT at the daily time step had NS values of 0.57 and 0.68, respectively, whereas the monthly NS values were 0.77 and 0.75, respectively. The  $\text{NO}_3^-$ -N and TP simulations by SWAT corresponded well to the observed timing of the events. However, modeled  $\text{NO}_3^-$ -N was overestimated by SWAT (PBIAS = 11.8%) and TP had overall lower simulated values (PBIAS 33.5%). The NS monthly calibration and validation values for  $\text{NO}_3^-$ -N were 0.77 and 0.72, respectively. For TP, the NS values were 0.47 and 0.52 for the calibration and validation, respectively. Based on the statistics and on the performance of the calibrated model, SWAT was able to satisfactorily simulate streamflow,  $\text{NO}_3^-$ -N, and TP in the watershed.

#### 3.3 Reference and future streamflow, $\text{NO}_3^-$ -N, and TP

The SWAT-simulated streamflow using each of the climate simulations for the future period was compared statistical-

ly ( $p < 0.05$ ) to the simulated streamflow using the climate simulations from the reference period (Table 2). The mean streamflow in September was simulated to be significantly lower in the future due to lower future precipitation in August, whereas in spring (April, May, and June), the mean streamflow was significantly higher caused by the greater amounts of precipitation throughout the winter and into the early spring months (Figure 3).

The long-term (1941–2008) average annual flow at the Treuchtlingen gauge was measured to be 5.73 m<sup>3</sup>/s, with daily flows ranging from a minimum 0.28 m<sup>3</sup>/s to a maximum 183 m<sup>3</sup>/s (BLFU, 2012). For the mid-term future, the simulated mean annual streamflow (5.44 m<sup>3</sup>/s) lies slightly under the historic average flow.

The monthly 10<sup>th</sup> percentile flows remain unchanged in the future. However, the simulated mean 90<sup>th</sup> percentile flows (statistically representing a 1 in 10-year event) are significantly lower in autumn (Table 3).

Higher mean values for the 90<sup>th</sup> percentile flows were simulated during the spring months (Tables 2 and 3).

Comparing the nutrient percentiles in each season between the simulated reference and future climate periods provides an indication of the changes due to possible future climates (Figures 4a and 4b). The simulated nutrient percentiles using the reference and future climates in SWAT were compared with the observed data from the reference time period (mean monthly values from 1975–2000) in the form of boxplots to indicate the deviation by the simulations from the observed data. Ideally, the median of the boxplot from using the reference climate simulations should lie on, or very near, the zero line to indicate no difference between the observed climate and the simulated reference climate outputs. Discrepancies in the simulated observed and simulated reference results are manifold and are due to the imperfect SWAT model setup, the chosen parameter values during the calibration, and due to the observed data. As well, in the climate models, the differences in parameters and in the representation of physical processes and different initial conditions from the members of the same model (i.e., ECM members 1, 2, and 3) will contribute to the spread of the simulated output results.

The SWAT model was able to capture the observed 90<sup>th</sup> percentile data well (depicted by the median nutrients in three out of the four seasons lying close to the zero line in Figure 4b), thus indicating greater confidence in the trend toward significantly higher 90<sup>th</sup> percentiles of  $\text{NO}_3^-$ -N loads in the future in the Altmühl. The future mean monthly  $\text{NO}_3^-$ -N loads are also simulated to be significantly higher in six months of the year (Table 4).

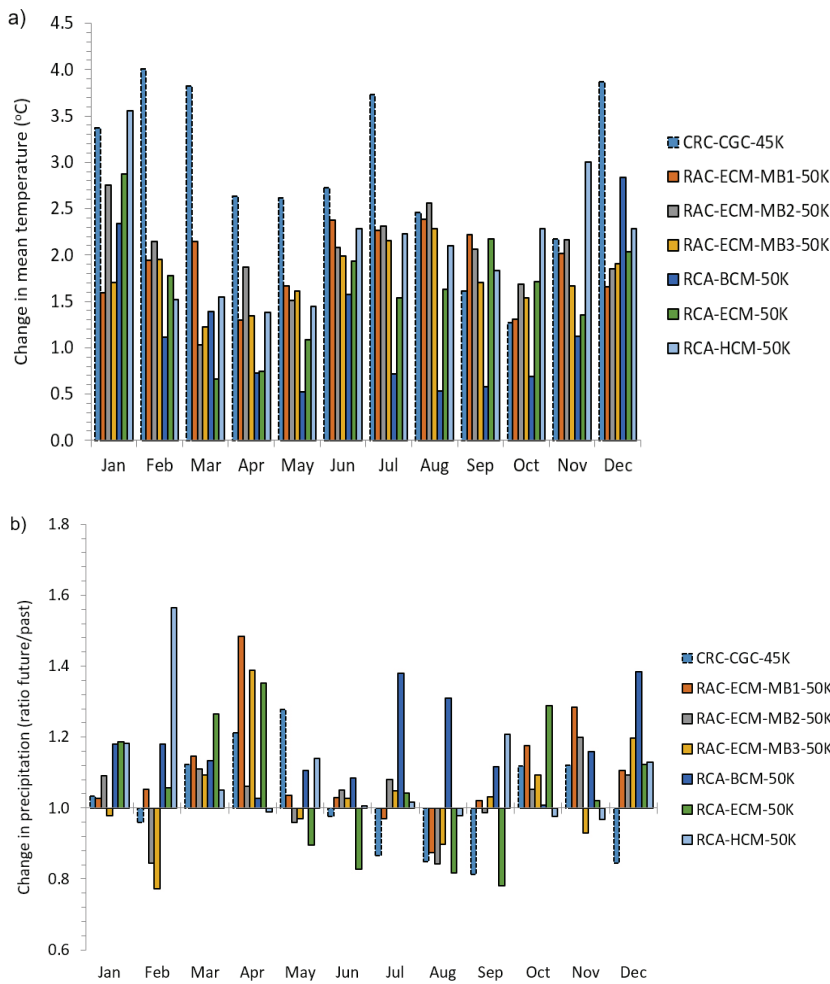


Figure 2. Future change in (a) mean temperature and (b) precipitation from bias-corrected climate model simulations (2041–2070), compared with the observed interpolated station data (1971–2000).

Abbildung 2. Zukünftige Änderungen der (a) mittleren Temperatur und (b) der Niederschläge aus Bias-korrigierten Klimasimulationen (2041-2070) im Vergleich mit beobachteten und interpolierten Stationsdaten (1971-2000).

In SWAT, the governing processes simulating  $\text{NO}_3^-$ -N loads transported from the field to the stream are dependent on soil mineralization and decomposition of the fresh organic pools and humus. Net mineralization occurs when the C:N is <20. Immobilization causes a net decrease in  $\text{NO}_3^-$ -N and occurs when the C:N is >30. All N mineralization algorithms in SWAT are net mineralization algorithms that consider immobilization into the equations. Net mineralization is dependent on the soil water availability in relation to the field capacity, and on soil temperature. When soil temperature (>0 °C) and water content increase, more nitrogen is mineralized and added to the soil nitrate pool.

In SWAT, the inputs from fresh organic pools (fertilizer or residue applications) are important sources of nitrogen; how-

ever, these pools were not altered during any of the model simulations. The average fertilizer applied to the cropland in the watershed was 67 kg N/ha/yr and 26 kg P/ha/yr, for both the reference and the future period, respectively.

Due to its negative charge, the  $\text{NO}_3^-$  molecule is not sorbed by the soil particles, rather it is soluble and can be carried over land in surface runoff, and it is readily transported by infiltration and lateral flow into the surface layers of the soil, as well as it can move upward in the soil in response to evaporation. April was the month with the highest increase in precipitation, yet May was the month when the difference in mean  $\text{NO}_3^-$ -N load was the largest (0.41 kg/ha) between the reference and the future period (Table 4); this is explained by the lag time for  $\text{NO}_3^-$ -N to be transported by the infiltrated water through the soil and into the river.

Denitrification removes  $\text{NO}_3^-$ -N from the soil under anaerobic conditions. In SWAT, when the water-filled pore space is  $>60\%$ , denitrification occurs. This process is also temperature-dependent, so higher soil temperatures ( $>0^\circ\text{C}$ ) coupled with anaerobic conditions enhance denitrification. However, denitrification did not cause any  $\text{NO}_3^-$ -N changes in the future simulations.

Plant growth also removes N from the soil during the growing season as a function of the growth stage. Due to the warmer growing season in the future climate, some crops (e.g., maize) extracted more nutrients from the soil to meet the growth needs, but this did not affect the 10<sup>th</sup> or 90<sup>th</sup> percentiles.

Phosphorus is much less mobile than nitrate. In SWAT, the P forms can be in solution and plant-available or they can be insoluble and bound to soil particles or precipitated out of solution.

Due to the low mobility of P, SWAT accounts for P in surface runoff and leachate only from the top 10 mm into the first soil layer. Organic and mineral P attached to the soil particles can be transported by surface runoff to the stream. This amount is associated with sediment loading.

For the mid-term future, the TP loads simulated during winter were diminished; this was depicted by the decreasing relative changes in the 10<sup>th</sup> and 90<sup>th</sup> percentiles, and also by the mean TP loads, which were all simulated to be significantly lower from December to February (Table 5 and Figure 5).

April and May mean TP loads and the spring 10<sup>th</sup> percentile were higher in the future (Figure 5 and Table 5), showing a shift toward fewer low events. The 10<sup>th</sup> percentile TP loads were well simulated, and therefore, indicate confidence in this trend.

TP loads in the reach were correlated ( $R^2 = 0.74$ ) to streamflow, so that the changes in TP seasonality followed the streamflow pattern closely. The months with the largest increases in flow compared with the reference period were April to June. The lowest flows occurred from August to February (Figure 3).

The 90<sup>th</sup> percentiles of TP loads decreased significantly in winter and otherwise remained statistically similar to the reference period.

Decomposition and mineralization of fresh organic residues and of the humus add plant-available P to the soil. These processes are controlled by the decay rate constant, which is determined in part by the soil temperature; warmer temperatures increase the decay rate.

For the future period, each month showed that the mean monthly temperature increased compared with the reference period. Warmer temperatures contribute to an accelerated mineralization of nutrients; this happened espe-

cially during the winter months when the soil temperature remained above  $0^\circ\text{C}$  more often.

By the mid-term future, at the outlet of the Altmühl watershed with a size of 99,335 ha, the simulated mean monthly median  $\text{NO}_3^-$ -N loads were 1.0 to 26.8 Mg higher than from 1975–2000; and simulated mean monthly median TP loads were up to 3.1 Mg lower.

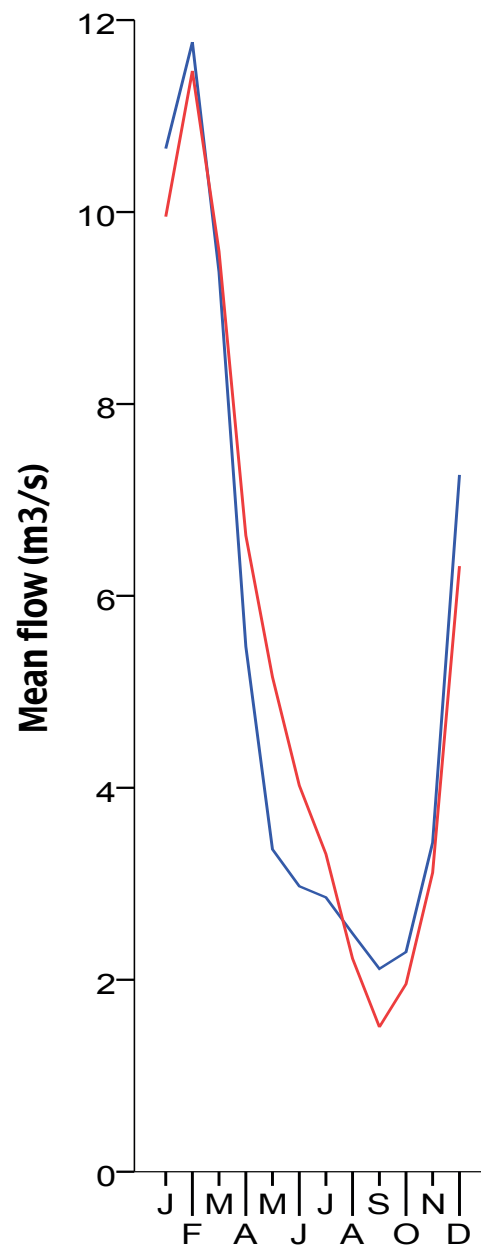


Figure 3. Mean monthly streamflow ( $\text{m}^3/\text{s}$ ) for the reference and the future period.

Abbildung 3. Mittlere monatliche Abflussdaten ( $\text{m}^3/\text{s}$ ) für die Referenz- und die Zukunftsperiode.

Table 2. Simulated streamflow (m<sup>3</sup>/s) at Treuchtlingen for 2046–2070 with the mean, standard deviation (std. dev.) and percentiles. Independent t-tests (p<0.05) compare the mean ( $\mu$ ) of the future climate simulations (2046–2070) to the mean of the reference climate simulations (1975–2000). An asterisk indicates a rejection of the null-hypothesis  $\mu_{\text{Ref}} = \mu_{\text{Fut}}$ , the value after the asterisk indicates the difference in m<sup>3</sup>/s. Tabelle 2. Simulierte Abflüsse (m<sup>3</sup>/s) am Pegel Treuchtlingen für den Zeitraum 2046-2070. Dargestellt sind Mittelwerte, Standardabweichungen und Perzentilen der Daten. Über unabhängige t-Tests (p<0.05) werden die Mittelwerte der Simulationen (2046-2070) mit denen der Referenzperiode (1975-2000) verglichen. Ein Asterisk bedeutet eine Ablehnung der Null-Hypothese  $\mu_{\text{Ref}} = \mu_{\text{Fut}}$ , der Wert nach dem Asterisk bezeichnet den Unterschied in m<sup>3</sup>/s.

Month	Future climate					Reference climate	t-test $\mu_0 = \mu_1$ (p<0.05)
	Mean	Std. dev.	Percentiles			Mean	
	$\mu_0$		10 <sup>th</sup>	50 <sup>th</sup>	90 <sup>th</sup>	$\mu_1$	
J	9.95	5.51	2.92	9.62	16.82	10.66	
F	11.47	5.74	4.48	10.95	19.09	11.77	
M	9.59	4.47	4.04	9.3	15.49	9.38	
A	6.63	4.12	2.10	5.78	12.54	5.47	*1.16
M	5.16	4.04	0.80	4.24	11.21	3.36	*1.8
J	4.02	3.71	0.74	2.59	9.47	2.98	*1.04
J	3.31	3.96	0.36	1.85	8.10	2.86	
A	2.22	2.51	0.24	1.22	5.81	2.48	
S	1.51	2.0	0.17	0.74	4.06	2.11	*-0.96
O	1.96	2.17	0.29	1.20	4.76	2.29	
N	3.12	2.93	0.38	2.09	6.54	3.43	
D	6.31	4.81	1.23	5.49	12.53	7.26	

Table 3. Simulated streamflow (m<sup>3</sup>/s) 10<sup>th</sup> and 90<sup>th</sup> percentiles by season at Treuchtlingen. Independent t-tests (p<0.05) comparing the reference climate simulations (1975–2000) with the future climate simulations (2046–2070). Different letters within a row denote significant differences (p<0.05). Tabelle 3. Die 10. und 90. Perzentile der simulierten Abflüsse (m<sup>3</sup>/s) differenziert nach Jahreszeiten am Pegel Treuchtlingen. Unabhängige t-Tests (p<0.05) vergleichen die Referenzperiode (1975-2000) mit den Simulationen (2046-2070). Verschiedene Buchstaben innerhalb einer Reihe kennzeichnen signifikante Unterschiede (p<0.05).

Season	Percentile	Reference climate (1975-2000)	Future climate (2046-2070)
DJF	10 <sup>th</sup>	3.1	2.2
	90 <sup>th</sup>	18.4	17.4
MAM	10 <sup>th</sup>	1.2	1.7
	90 <sup>th</sup>	11.5 b	13.4 a
JJA	10 <sup>th</sup>	0.4	0.4
	90 <sup>th</sup>	6.5	7.6
SON	10 <sup>th</sup>	0.2	0.3
	90 <sup>th</sup>	7.0 a	5.4 b

The 90<sup>th</sup> percentile increase in the future streamflow in spring did not consistently increase in the 90<sup>th</sup> percentiles of the nutrient simulations. The lower 10<sup>th</sup> percentile in autumn for flow also had no impact on the nutrients 10<sup>th</sup> percentiles. Very high nutrient loads are usually due to a combination of high precipitation events with a field management practice, such as fertilization. Very low nutrient

loads can be due to low precipitation, combined with rapid plant growth. The dynamics of TP and NO<sub>3</sub><sup>-</sup>-N transport, are therefore, better described using smaller time steps. Nitrate can be transported after a precipitation event through several pathways (infiltration, lateral flow, surface runoff) and end up within hours or days in the stream, whereas TP is mainly transported by surface runoff and in-

Table 4. Simulated nitrate nitrogen loads (kg/ha) at Treuchtlingen for 2046–2070 with the mean, standard deviation (std. dev.) and percentiles. Independent t-tests ( $p < 0.05$ ) compare the mean ( $\mu$ ) of the future climate simulations to the mean of the reference climate simulations (1975–2000). An asterisk indicates a rejection of the null-hypothesis  $\mu_{\text{Ref}} = \mu_{\text{Fut}}$ , the value after the asterisk indicates the difference in kg/ha. Tabelle 4. Die simulierten Nitrat-Stickstoff-Frachten (kg/ha) am Pegel Treuchtlingen für den Zeitraum 2046-2070 mit dem dazugehörigen Mittelwerten, Standardabweichungen und Perzentilen. Über unabhängige t-Tests ( $p < 0.05$ ) werden die Mittelwerte der Simulationen (2046-2070) mit denen der Referenzperiode (1975-2000) verglichen. Ein Asterisk bedeutet eine Ablehnung der Null-Hypothese  $\mu_{\text{Ref}} = \mu_{\text{Fut}}$ , der Wert nach dem Asterisk bezeichnet den Unterschied in kg/ha.

Month	Future climate					Reference climate	t-test $\mu_0 = \mu_1$ ( $p < 0.05$ )
	Mean $\mu_0$	Std. dev.	Percentiles			Mean $\mu_1$	
			10 <sup>th</sup>	50 <sup>th</sup>	90 <sup>th</sup>		
J	2.47	1.40	0.96	2.28	4.28	2.18	*0.29
F	2.23	1.02	1.00	2.12	3.48	2.11	
M	2.02	1.09	0.83	1.91	3.17	1.99	
A	1.26	1.10	0.25	0.99	2.70	1.05	
M	0.87	1.14	0.07	0.40	2.46	0.47	*0.41
J	0.51	0.83	0.05	0.19	1.48	0.28	*0.23
J	0.45	0.89	0.02	0.12	1.28	0.24	*0.21
A	0.36	0.63	0.01	0.08	1.12	0.27	
S	0.34	0.54	0.01	0.07	1.29	0.34	
O	0.70	0.88	0.03	0.39	1.78	0.49	*0.21
N	1.09	0.90	0.08	0.91	2.48	0.79	*0.30
D	1.82	1.23	0.49	1.56	3.33	1.61	

Table 5. Simulated total phosphorus loads (kg/ha) at Treuchtlingen for 2046–2070 with the mean, standard deviation (std. dev.) and percentiles. Independent t-tests ( $p < 0.05$ ) compare the mean ( $\mu$ ) of the future climate simulations to the mean of the reference climate simulations (1975–2000). An asterisk indicates a rejection of the null-hypothesis  $\mu_{\text{Ref}} = \mu_{\text{Fut}}$ , the value after the asterisk indicates the difference in kg/ha. Tabelle 5. Die simulierten Gesamtphosphor-Frachten (kg/ha) am Pegel Treuchtlingen für den Zeitraum 2046-2070 mit dem dazugehörigen Mittelwerten, Standardabweichungen und Perzentilen. Über unabhängige t-Tests ( $p < 0.05$ ) werden die Mittelwerte der Simulationen (2046-2070) mit denen der Referenzperiode (1975-2000) verglichen. Ein Asterisk bedeutet eine Ablehnung der Null-Hypothese  $\mu_{\text{Ref}} = \mu_{\text{Fut}}$ , der Wert nach dem Asterisk bezeichnet den Unterschied in kg/ha.

Month	Future climate					Reference climate	t-test $\mu_0 = \mu_1$ ( $p < 0.05$ )
	Mean $\mu_0$	Std. dev.	Percentiles			Mean $\mu_1$	
			10 <sup>th</sup>	50 <sup>th</sup>	90 <sup>th</sup>		
J	0.084	0.080	0.011	0.059	0.191	0.144	*-0.06
F	0.089	0.103	0.004	0.049	0.241	0.133	*-0.04
M	0.044	0.047	0.007	0.029	0.096	0.073	*-0.03
A	0.038	0.039	0.007	0.029	0.082	0.026	*0.015
M	0.042	0.040	0.009	0.029	0.101	0.028	*0.014
J	0.033	0.033	0.005	0.021	0.086	0.027	
J	0.024	0.031	0.004	0.015	0.050	0.023	
A	0.015	0.018	0.002	0.008	0.038	0.016	
S	0.011	0.016	0.001	0.006	0.021	0.014	
O	0.015	0.018	0.001	0.010	0.031	0.013	
N	0.021	0.030	0.002	0.011	0.049	0.020	
D	0.060	0.073	0.005	0.031	0.163	0.079	*-0.02

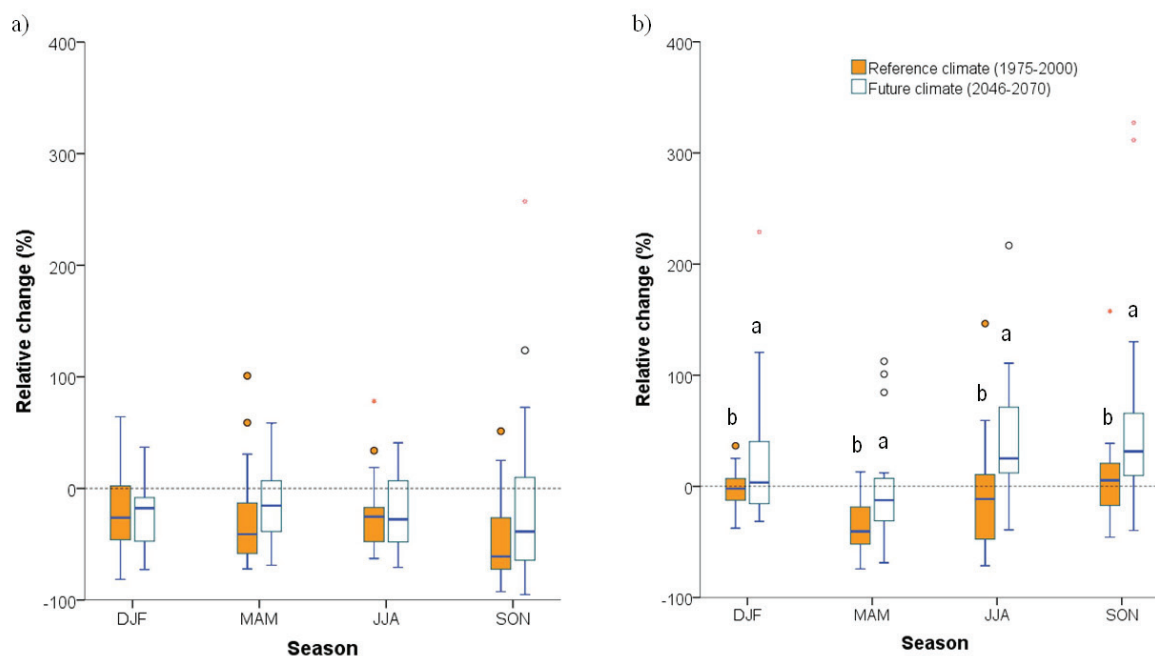


Figure 4. Relative changes (%) to the seasonal mean observed data from 1975–2000 (zero line) in (a) 10<sup>th</sup> percentiles and (b) 90<sup>th</sup> percentiles for nitrate nitrogen loads at Treuchtlingen. The boxplots show the side-by-side comparisons between SWAT simulated with the reference climate (orange boxes) and with future climate data (white boxes). The difference between the orange and white boxes is the climate change signal. The letters denote statistically significant ( $p < 0.05$ ) differences between the reference climate and the future climate.

Abbildung 4. Die relativen Änderungen (%) der (a) 10. und (b) 90. Perzentile für die mittleren, saisonalen gemessenen Nitrat-Stickstoff Frachten von 1975-2000 (Null-Linie) am Pegel Treuchtlingen. Die Boxplots stellen den Vergleich der Referenzperiode (orangene Farbe) mit den Simulationen für die Zukunft (weiße Farbe) dar. Der Unterschied zwischen den Beiden gibt das Klimawandelsignal an. Die Buchstaben kennzeichnen statistisch signifikante ( $p < 0.05$ ) Unterschiede zwischen der Referenz- und der Zukunftsperiode.

teracts with the top 10 mm of the soil. The transported TP is sorbed to sediments and is transported by erosion or surface runoff processes, which take longer to travel because the particulate P can be deposited and eventually never make it to the stream. TP is more correlated to streamflow and high surface runoff events than  $\text{NO}_3^-$ -N loads are.

#### 4. Conclusion

In the future mid-term horizon, the 90<sup>th</sup> percentiles of streamflow were lower than the reference simulations in autumn, indicating a shift in the hydrograph toward less high flow periods and longer low flow periods throughout the summer and into autumn. The simulated higher future 90<sup>th</sup> percentiles from March to May indicate a tendency toward greater streamflow, caused by the higher precipitation received in spring. The intensity of the precipitation events could not be verified as daily precipitation data was used.

The simulated significant increase in the 90<sup>th</sup> percentile  $\text{NO}_3^-$ -N loads in all seasons in the future indicates that the right-hand tail of  $\text{NO}_3^-$ -N transport is simulated to be higher in the future. The increases in the 90<sup>th</sup> percentile  $\text{NO}_3^-$ -N load events in the future should be addressed through best field measures.

The 90<sup>th</sup> percentile TP load events will diminish or remain similar to the reference period, and therefore, not pose more challenges than they do currently. The TP loads in winter will be more centered around the mean, shown by both the higher 10<sup>th</sup> and the lower 90<sup>th</sup> percentiles in winter.

Climate change will affect the extreme events related to streamflow and also to nutrient load transport, such as for  $\text{NO}_3^-$ -N, and TP. This study represents one setup of the SWAT model in which the land use was considered to be static for the simulation period. If agricultural land use changes, then the nutrient inputs from fertilizer may also vary spatially and in the amounts applied which will affect the results.

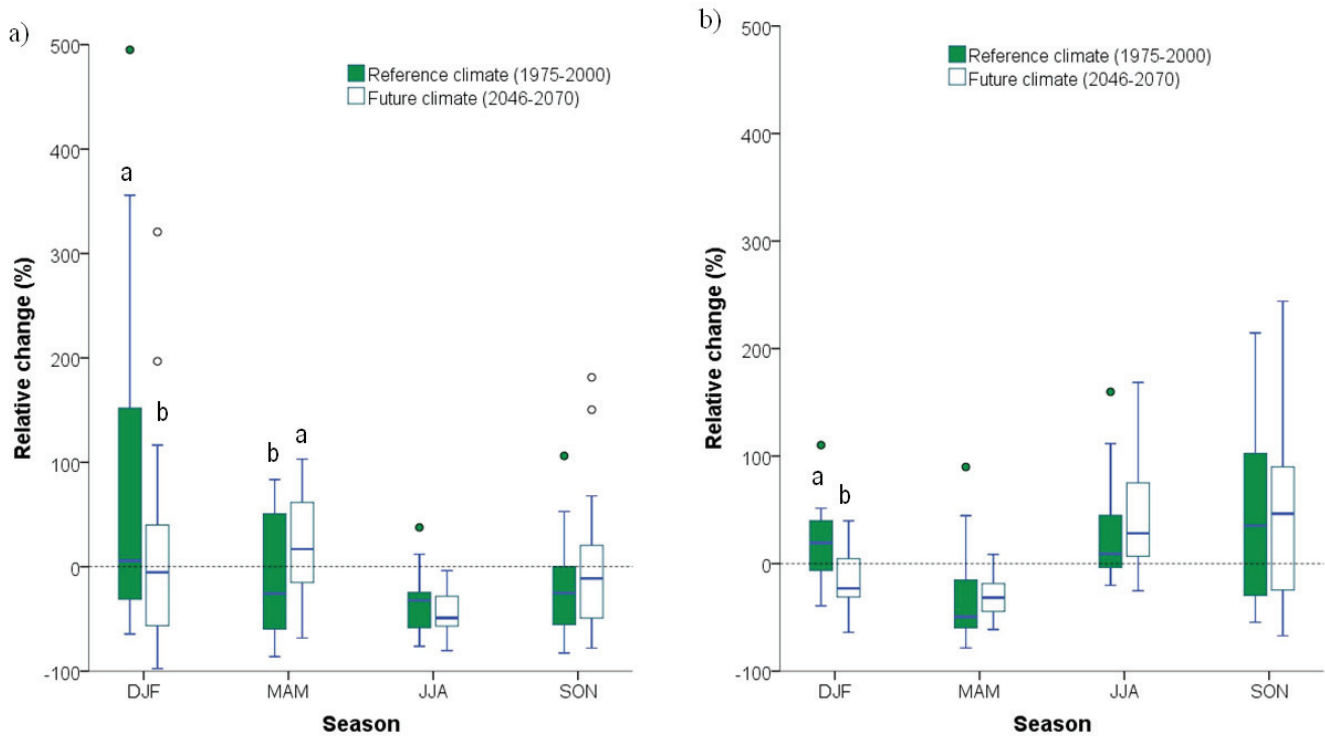


Figure 5. Relative changes (%) to the seasonal mean observed data from 1975–2000 (zero line) in (a) 10<sup>th</sup> percentiles and (b) 90<sup>th</sup> percentiles for total phosphorus loads at Treuchtingen. The boxplots show the side-by-side comparisons between SWAT simulated with the reference climate (green boxes) and with future climate data (white boxes). The difference between the green and white boxes is the climate change signal. The letters denote statistically significant ( $p < 0.05$ ) differences between the reference climate and the future climate.

Abbildung 5. Die relativen Änderungen (%) der (a) 10. und (b) 90. Perzentile für die mittleren, saisonalen gemessenen Gesamtphosphor-Frachten von 1975-2000 (Null-Linie) am Pegel Treuchtingen. Die Boxplots stellen den Vergleich der Referenzperiode (grüne Farbe) mit den Simulationen für die Zukunft (weiße Farbe) dar. Der Unterschied zwischen den Beiden gibt das Klimasignal an. Die Buchstaben kennzeichnen statistisch signifikante ( $p < 0.05$ ) Unterschiede zwischen der Referenz- und der Zukunftsperiode.

## Acknowledgements

This work was partially supported by the Natural Sciences and Engineering Research Council of Canada, and funds from the Bourses Québec-Bavière.

## References

- Abbaspour, K.C. (2011): SWAT-CUP4: SWAT Calibration and Uncertainty Programs - A User Manual. Swiss Federal Institute of Aquatic Science and Technology, Eawag, Dübendorf, Switzerland, 103 pp.
- Abbaspour, K.C., Johnson, C.A. and M.T. van Genuchten (2004): Estimating uncertain flow and transport parameters using a sequential uncertainty fitting procedure. *Vadose Zone Journal* 3, 1340–1352.
- Arnold, J.G. and P.M. Allen (1999): Automated methods for estimating baseflow and ground water recharge from streamflow records. *Journal of the American Water Resources Association* 35, 411–424.
- Arnold, J.G., Moriasi, D.N., Gassman, P.W., Abbaspour, K.C., White, M.J., Srinivasan, R., Santhi, C., Harmel, R.D., van Griensven, A., van Liew, M.W., Kannan, N. and M.K. Jha (2012): SWAT: Model use, calibration, and validation. *Transactions of the ASABE* 55, 1491–1508.
- Arnold, J.G., Srinivasan, R., Mutiah, R.S. and J.R. Williams (1998): Large area hydrologic modeling and assessment part I: Model development. *Journal of the American Water Resources Association* 34, 73–89.

- Behrendt, H. and D. Opitz (2000): Retention of nutrients in river systems: Dependence on specific runoff and hydraulic load. *Hydrobiologia* 410, 111–122.
- BLfU (2012): Hochwassernachrichtendienst. [www.hnd.bayern.de](http://www.hnd.bayern.de). Accessed on December 6 2012.
- BMLU (2002): Bavaria land of water: Sustainable water management in Bavaria. Bavarian State Ministry for Regional Development and Environmental Affairs, Munich, Germany, 94 pp.
- Deutscher Wetterdienst (2011): Daten der synoptischen Klimastationen. [www.dwd.de/bvbw/appmanager/bvbw](http://www.dwd.de/bvbw/appmanager/bvbw).
- EC (2000): European Commission Directive 2000/60/EC of the European Parliament and of the council of 23 October 2000 establishing a framework for Community action in the field of water policy. *Official Journal of the European Community* 22 L 327/1, pp. 72.
- Gassman, P.W., Reyes, M.R., Green, C.H. and J.G. Arnold (2007): The Soil and Water Assessment Tool: Historical development, applications, and future research directions. *Transactions of the ASABE* 50, 1211–1250.
- Hancock, G.R. (2012): Modelling stream sediment concentration: An assessment of enhanced rainfall and storm frequency. *Journal of Hydrology* 430–431, 1–12.
- Kovats, R.S., Valentini, R., Bouwer, L.M., Georgopoulou, E., Jacob, D., Martin, E., Rounsevell, M. and J.-F. Soussana (2014): Europe. In: Field, C.B., Barros, V.R., Dokken, D.J., Mastrandrea, M.D., Mach, K.J. Bilir, T.E., Chatterjee, M., Ebi, K.L., Estrada, Y.O., Genova, R.C., Girma, B., Kissel, E.S., Levy, A.N., MacCracken, S., Mastrandrea P.R. and L.L. White (Eds.): *Climate Change 2014: Impacts, Adaptation, and Vulnerability. Part B: Regional Aspects. Contribution of Working Group II to the Fifth Assessment Report of the Intergovernmental Panel on Climate Change*. Cambridge University Press, Cambridge, United Kingdom and New York, NY, USA, pp. 1267–1326.
- KTBL (1995): Betriebsplanung 1995/1996: Daten für die Betriebsplanung in der Landwirtschaft. Kuratorium für Technik und Bauwesen in der Landwirtschaft e.V. (KTBL), Darmstadt, 182 pp.
- KTBL (2009): *Faustzahlen für die Landwirtschaft*. 14. Auflage, Kuratorium für Technik und Bauwesen in der Landwirtschaft e.V. (KTBL), Darmstadt, 1180 pp.
- Marke, T. (2008): Development and Application of a Model Interface to couple Land Surface Models with Regional Climate Models for Climate Change Risk Assessment in the Upper Danube Watershed. PhD Thesis, Ludwig Maximilians University, Munich, Germany, 220 pp.
- Mehdi, B., Ludwig, R. and B. Lehner (2015): Evaluating the impacts of climate change and crop land use change on streamflow, nitrates and phosphorus: A modeling study in Bavaria. *Journal of Hydrology: Regional Studies* 4, 60–90.
- Michael, A., Schmidt, J., Enke, W., Deutschländer, T. and G. Malitz (2005): Impact of expected increase in precipitation intensities on soil loss – results of comparative model simulations. *Catena* 61, 155–164.
- Moriasi, D.N., Arnold, J.G., Van Liew, M.W., Bingner, R.L., Harmel, R.D. and T.L. Veith (2007): Model evaluation guidelines for systematic quantification of accuracy in watershed simulations. *Transactions of the ASABE* 50, 885–900.
- Muerth, M.B., Gauvin St-Denis, B., Ricard, S., Velázquez, J.A., Schmid, J., Minville, M., Caya D., Chaumont, D., Ludwig, R. and R. Turcotte (2013): On the need for bias correction in regional climate scenarios to assess climate change impacts on river runoff. *Hydrology and Earth System Sciences* 17, 1189–1204.
- Muerth, M. (2008): A soil temperature and energy balance model for integrated assessment of Global Change impacts at the regional scale. PhD Thesis, Ludwig Maximilians University, Munich, Germany, 145 pp.
- Nakicenovic, N., Alcamo, J., Davis, G., de Vries, B., Fenhann, J., Gaffin, S., Gregory, K., Grübler, A., Jung, T.J., Kram, T., La Rovere, E.L., Michaelis, L., Mori, S., Morita, T., Pepper, W., Pitcher, H., Price, L., Riahi, K., Roehrl, A., Rogner, H.-H., Sankovski, A., Schlesinger, M., Shukla, P., Smith, S., Swart, R., van Rooijen, S., Victor, N. and Z. Dadi (2000): *Emission Scenarios. A special report of working group III of the Intergovernmental Panel on Climate Change*. Cambridge University Press, Cambridge, UK, 599 pp.
- Neitsch, S.L., Arnold, J.G., Kiniry, J.R. and J.R. Williams (2011): *Soil and water assessment tool theoretical documentation, Version 2009*. Technical Report No. 406, Texas Water Resources Institute, Texas, 647 pp.
- Radermacher, C. and L. Tomassini (2012): Thermodynamic causes for future trends in heavy precipitation over Europe based on an ensemble of regional climate model simulations. *Journal of Climate* 25, 7669–7689.
- Ramos, M.C. and J.A. Martínez-Casasnovas (2009): Impacts of annual precipitation extremes on soil and nutrient losses in vineyards of NE Spain. *Hydrological Processes* 23, 224–235.
- Schmidli, J., Frei, C. and P.L. Vidale (2006): Downscaling from GCM precipitation: A benchmark for dynamical and statistical downscaling methods. *International Journal of Climatology* 26, 679–689.

- Schrenk-Bergt, C., Krause, D., Prawitt, O., Lewandowski, J. and C.E.W. Steinberg (2004): Eutrophication problems and their potential solutions in the artificial shallow Lake Altmühlsee (Germany). *Studia Quaternaria* 21, 73–86.
- StLfW (1996): Gewässerkunde: Hydrologische Planungsgrundlagen Periode 1961-1990, Karten zur Wasserwirtschaft. Bayerisches Landesamt für Wasserwirtschaft, Munich, Germany.
- USDA (1972): USDA Soil Conservation Service. National Engineering Handbook, Hydrology, Section 4, Chapters 4–10. GPO, Washington, DC.
- Velázquez, J.A., Schmid, J., Ricard, S., Muerth, M., Gauvin St-Denis, B., Minville, M., Chaumont, D., Caya, D., Ludwig, R. and R. Turcotte (2013): An ensemble approach to assess hydrological models' contribution to uncertainties in the analysis of climate change impact on water resources. *Hydrology and Earth System Sciences* 17, 565–578.
- Wendland, M., Diepolder, M. and P. Capriel (2011): Leitfaden für die Düngung von Acker- und Grünland. 9. unveränderte Auflage, Gelbes Heft, Bayerische Landesanstalt für Landwirtschaft, Freising-Weihenstephan, 99 pp.
- Williams, J.R., Jones, C.A. and P.T. Dyke (1984): A modelling approach to determining the relationship between erosion and soil productivity. *Transactions of the American Society of Agricultural Engineers* 27, 129–144.
- Zolina, O., Simmer, C., Kapala, A., Bachner, S., Gulev, S. and H. Maechel (2008): Seasonally dependent changes of precipitation extremes over Germany since 1950 from a very dense observational network. *Journal of Geophysical Research: Atmospheres* 113, D06110.